Atmos. Chem. Phys. Discuss., 9, 14601–14643, 2009
www.atmos-chem-phys-discuss.net/9/14601/2009/

Atmospheric Chemistry and Physics Discussions

This discussion paper is/has been under review for the journal *Atmospheric Chemistry and Physics (ACP)*. Please refer to the corresponding final paper in *ACP* if available.

Planetary wave activity in the Arctic and Antarctic lower stratospheres during 2007 and 2008

S. P. Alexander[1] **and M. G. Shepherd**[2]

[1]Australian Antarctic Division, Kingston, Tasmania, Australia
[2]Centre for Research in Earth and Space Science, York University, Toronto, Canada

Received: 28 May 2009 – Accepted: 25 June 2009 – Published: 7 July 2009

Correspondence to: S. P. Alexander (simon.alexander@aad.gov.au)

Published by Copernicus Publications on behalf of the European Geosciences Union.

Abstract

Temperature data from the COSMIC GPS-RO satellite constellation are used to study planetary wave activity in both polar stratospheres from September 2006 until November 2008. One major and several minor sudden stratospheric warmings (SSWs) were recorded during the boreal winters of 2006/2007 and 2007/2008. Planetary wave morphology is studied using space-time spectral analysis while individual waves are extracted using a linear least squares fitting technique. Results show the planetary wave frequency and zonal wavenumber distribution varying between hemisphere and altitude. Most of the large Northern Hemisphere wave activity is associated with the winter SSWs, while the largest amplitude waves in the Southern Hemisphere occur during spring. Planetary wave activity during the 2006/2007 and 2007/2008 Arctic SSWs is due largely to travelling waves with zonal wavenumbers $|s|=1$ and $|s|=2$ having periods of 12, 16 and 23 days and stationary waves with $s=1$ and $s=2$. The latitudinal variation of wave amplification during the two Northern Hemisphere winters is studied. Most planetary waves show different structure and behaviour during each winter. Abrupt changes in the latitude of maximum amplitude of some planetary waves is observed co-incident in time with some of the SSWs.

1 Introduction

Large amplitude planetary waves dominate the winter middle atmosphere and their interaction with the zonal mean flow is a major driver of winter stratosphere dynamics (Andrews et al., 1987). Planetary wave amplitudes are larger in the Northern Hemisphere than in the Southern Hemisphere due to larger themal and orographic forcing (Andrews et al., 1987). Stratospheric waves generally propagate eastward relative to the ground in the Southern Hemisphere (Hartmann et al., 1984; Shiotani et al., 1990), while quasi-stationary waves dominate the Northern Hemisphere (Chshyolkova et al., 2005). However, planetary waves generally propagate westward relative to the zonal

ACPD

9, 14601–14643, 2009

mean flow (Holton, 2004).

Planetary waves propagate upward from tropospheric sources (Hartmann et al., 1984; Randel, 1987; Krüger et al., 2005). Several studies have shown the connection between tropospheric and stratospheric planetary wave activity. Leovy and Webster (1976) and Mechoso and Hartmann (1982) discussed the strong vertical coherence of travelling planetary waves. Randel (1987) used geopotential height below 1 hPa to find a decrease in propagation time from the troposphere to stratosphere for higher zonal wavenumber waves. Westward propagating waves with zonal wavenumber s=1 and s=2 were identified in the stratosphere using satellite data and shown to agree with Rossby modes for an isothermal atmosphere (Hirota and Hirooka, 1984). Recent satellite datasets have enabled wave characteristics and propagation to be followed up to the mesosphere and lower thermosphere (Hirooka, 2000; Palo et al., 2005).

Sudden stratospheric warmings (SSWs) are much more prevalent in the Arctic than in the Antarctic due to the larger Northern Hemisphere planetary wave forcing (Manney et al., 2005; Pancheva et al., 2008a). Indeed, only one major SSW has been recorded in the Antarctic, during spring 2002 (Newman and Nash, 2005). An increase in middle atmospheric planetary wave activity is noticed prior to the onset of an SSW which preconditions the atmosphere (e.g. Palo et al., 2005; Chshyolkova et al., 2006; Hoffmann et al., 2007), leading to an upward and poleward motion of heat flux (Andrews et al., 1987). Planetary waves interact dramatically with the background mean flow during the SSW, leading to a reversal of the meridional temperature gradient at 10 hPa for minor warmings and additionally for major warmings, a reversal of the eastward flow (Labitzke and Naujokat, 2000). Matsuno (1971) showed that SSWs can be explained by the interaction of upward propagating transient planetary waves on the background zonal mean flow. A downward circulation causing adiabatic heating in the stratosphere results from the deceleration of the eastward flow by planetary waves (Liu and Roble, 2002).

The stratosphere-mesosphere system is coupled via planetary wave propagation during SSWs (Liu and Roble, 2005; Hoffmann et al., 2007; Pancheva et al., 2009a),

ACPD
9, 14601–14643, 2009

which act to change the stratopause structure (Manney et al., 2008) and the nature of waves in the mesosphere (Chshyolkova et al., 2006; Shepherd et al., 2007; Murphy et al., 2007; Pancheva et al., 2008b). During the austral winter of 2002, multiple planetary waves reached the mesosphere, weakening and eventually reversing the polar night jet, thus changing wave transmission and breaking conditions (Krüger et al., 2005; Liu and Roble, 2005). SSWs alter the background stratospheric circulation and thereby influence directly the gravity wave fluxes reaching the mesosphere. The westward winds observed during major SSWs allow eastward propagating gravity waves to reach the MLT region and deposit their momentum there (Dunkerton and Butchart, 1984). Gravity wave activity in the stratosphere is generally enhanced during SSWs (Duck et al., 1998; Ratnam et al., 2004; Alexander et al., 2009), although in the mesosphere, gravity wave activity depends upon the warming itself and the location of the observations (Dowdy et al., 2007; Hoffmann et al., 2007).

The recent advent of GPS Radio Occultation (RO) satellite missions has resulted in the collection of highly accurate (sub-Kelvin accuracy) and increasingly dense temperature profiles from near the surface to 40 km altitude (Kursinski et al., 1997; Tsuda et al., 2000). The launch of the Constellation Observing System for Meteorology, Ionosphere and Climate Global Positioning System Radio Occultation (COSMIC GPS-RO) satellites in April 2006 has resulted in towards 2000 profiles per day distributed about the globe (Anthes et al., 2008). These profiles are distributed fully in longitude and local time, making them ideal for global scale wave studies (Alexander et al., 2008b). COSMIC data were used to show large planetary wave activity in the 2006 Antarctic early summer, more consistent with winter-time activity (Shepherd and Tsuda, 2008). COSMIC data are also dense enough to quantify changes in gravity wave activity over short time scales (on the order of several days) and in particular have been used to study gravity wave activity associated with recent Arctic SSWs (Alexander et al., 2009).

In this paper, we study planetary wave activity using COSMIC temperature data between 15 km and 35 km altitude from September 2006 to November 2008. We use two methods to study planetary waves in the Arctic (60° N–70° N) and Antarctic (60° S–

ACPD
9, 14601–14643, 2009

70° S). Firstly, space-time spectral analysis provides a morphology of planetary waves during this period and allows quantification and analysis of travelling and stationary wave components. Wave periods, wave numbers and phase speeds are examined. Then we extract individual waves from the temperature perturbations using a least squares fitting method. From this we look at the height structure and periods of these waves through time. Lastly, we identify individual waves and study their latitudinal distribution during the major and minor sudden stratospheric warmings of the Arctic winters of 2006/2007 and 2007/2008.

2 Data analysis

2.1 COSMIC data

The COSMIC version 2.0 dry temperature data product is used, which is derived from the measured refractivity profile by neglecting humidity. Sufficient data for this analysis are available from September 2006 onwards. The original GPS-RO data are available at 0.1 km vertical resolution but they have an effective vertical resolution on the order of 1 km in the lower stratosphere (Kursinski et al., 1997). Therefore the data are interpolated to the approximate real resolution of 1 km. The precision of the COSMIC refractivity is 0.7% at 30 km (Schreiner et al., 2007). The accuracy of the derived temperature is better than 0.5 K (Kursinski et al., 1997). Only a small bias of 1–2% between radiosondes and COSMIC at 25 km altitude was observed by Hayashi et al. (2009), thus gravity wave and planetary wave activity observed with COSMIC agrees well with model results (Alexander et al., 2008a,b; Kawatani et al., 2009). COSMIC data are available from near the surface to 40 km, although we consider altitudes 15 km–35 km here to neglect humidity in the lower regions and to maintain accuracy at the upper altitudes.

ACPD
9, 14601–14643, 2009

2.2 Space-time power spectral analysis

The space-time spectral analysis method is a technique for studying planetary scale waves in the atmosphere (Hayashi, 1971). This method allows the simultaneous separation of the background field into eastward and westward propagating waves. Space-time analysis has been used to study planetary waves from the mid-latitude surface to middle stratosphere (e.g. Mechoso and Hartmann, 1982; Speth and Madden, 1983; Hirota and Hirooka, 1984; Hirooka and Hirota, 1985; Watanabe et al., 2008) and globally in the MLT region (e.g. Garcia et al., 2005; Palo et al., 2007; Ern et al., 2009). Global scale stratospheric equatorial waves such as Kelvin waves and mixed Rossby-gravity waves have also been studied using this method (Wheeler and Kiladis, 1999; Randel and Wu, 2005; Alexander et al., 2008b; Ern et al., 2008).

For a fixed latitude, the temperature T, which is a function of longitude λ and time t, can be expressed as a double Fourier expansion:

$$T(\lambda, t) = \sum_{s} \sum_{\pm\omega} R_{s,\pm\omega} \cos(s\lambda \pm \omega t + \phi_{s,\pm\omega}) \quad (1)$$

where $R_{s,\pm\omega}$ is the amplitude, s is the zonal wavenumber, ω is the frequency and ϕ is the phase. The positive and negative signs correspond to eastward and westward propagating waves respectively. The space-time power spectrum is given by (Hayashi, 1971):

$$P_{s,\pm\omega}(T) = \sum_{\Delta\omega} \frac{1}{2} R_{s,\pm\omega} \quad (2)$$

where $\Delta\omega$ indicates the summation over a particular frequency band. Practically, the $R_{s,\pm\omega}$ and $\phi_{s,\pm\omega}$ are obtained by taking the FFT in longitude:

$$T(\lambda, t) = \sum_{s} C_s(t) \cos(s\lambda) + S_s(t) \sin(s\lambda) \quad (3)$$

ACPD
9, 14601–14643, 2009

and using these Fourier coefficients as input for further FFTs in time:

$$C_s(t) = \sum_{\omega} A_{s,\omega} \cos(\omega t) + B_{s,\omega} \sin(\omega t) \quad (4)$$

$$S_s(t) = \sum_{\omega} a_{s,\omega} \cos(\omega t) + b_{s,\omega} \sin(\omega t) \quad (5)$$

where the co-efficients $A_{s,\omega}$, $B_{s,\omega}$, $a_{s,\omega}$ and $b_{s,\omega}$ can be related to $R_{s,\pm\omega}$ and $\phi_{s,\pm\omega}$ (the reader is referred to Hayashi (1971) for full details).

There is significant stationary wave activity in the mid-latitudes. The standing (stationary) part of the variance can be shown to be (Hayashi, 1977):

$$Y_{s,\omega}(T) = \left(\frac{1}{4}[P_{\omega}(C_s) - P_{\omega}(S_s)] + K^2_{\omega}(C_k S_s)\right)^{\frac{1}{2}} \quad (6)$$

where K_{ω} is the co-spectrum. The travelling components are then given by:

$$Z_{s,\pm\omega}(T) = P_{s,\pm\omega}(T) - \frac{1}{2} Y_{s,\omega}(T) \quad (7)$$

As discussed by Hayashi (1982), the partitioning of spectra into travelling and standing wave components is based on the following assumptions and definitions:

1. The definition of the standing wave component is that part of the spectrum which consists of coherent eastward and westward moving components which are of equal amplitude.
2. The definition of the traveling wave component is that part of the spectrum consisting of eastward and westward moving components which are incoherent with each other.
3. It is assumed that standing and traveling parts are incoherent with each other and of different origin.

2.3 Planetary wave extraction

The space-time analysis provides a detailed overview of the contribution to the variance of planetary waves with different frequencies, wavenumbers and phase velocities. However, the removal of the stationary wave components via Eqs. (6) and 7 leads to an irreversible loss of the Fourier coefficients such that individual travelling planetary waves are unable to be recovered.

The large stationary wave activity may distort the often weaker travelling waves if they are not considered simultaneously. Therefore, we extract individual planetary waves in longitude and time by the simultaneous least-squares fitting of stationary and travelling waves to the function (Pancheva et al., 2008b; Shepherd and Tsuda, 2008):

$$T_m = T_0 + \sum_{j=1}^{6} \sum_{s=-3}^{3} A_{s,j} \cos\left(\frac{2\pi}{\tau_j} t - \frac{2\pi}{360} s\lambda - \psi_{s,j}\right) + \sum_{s=1}^{3} B_s \cos\left(\frac{2\pi}{360} s\lambda - \phi_s\right) + R \quad (8)$$

where T_m is the modelled temperature, T_0 the background temperature field, t is time in days counting from t=0 on 1 September 2006 and R is the residual containing all other wave periods, wavenumbers and noise. The first summation on the right hand side of Eq. (8) is the time-dependent travelling wave component, with amplitudes $A_{s,j}$ and phases $\psi_{s,j}$, while the second summation is the stationary wave component with amplitudes B_s and phases ϕ_s.

The ground-based wave periods τ are determined from an initial wavelet analysis of the eastward and westward components of $|s|\leq 3$ planetary waves (which are a combination of stationary and travelling waves) extracted from the s–ω analysis. The main τ are found to be 5, 8, 10, 12, 16 and 23 days, although the 5 day and 8 day waves are generally quite small in amplitude. These periods are in good agreement with previous

ACPD
9, 14601–14643, 2009

observations of planetary wave periods (Pancheva et al., 2008b, 2009a). The analysis period is 46 days (twice the longest τ under consideration) and the least-squares fitting is stepped forward in time by one day intervals. Positive s corresponds to eastward propagating waves, while negative s corresponds to westward propagating waves. The reconstructed model data only requires $|s| \leq 2$ to agree closely with the original COSMIC temperature perturbations. We do not require the s=0 zonally symmetric waves to obtain good model agreements (Shepherd and Tsuda, 2008), although these waves are likely to be important at higher altitudes (Pancheva et al., 2007). The sum of the amplitudes of R and waves with $|s|$=3 and s=0 (which are not needed in the reconstruction) are insignificant. The wave phases $\psi_{s,i}$ and ϕ_s are not considered further because of the limited altitude range of COSMIC data when compared to the vertical wavelengths of planetary waves which are several tens of kilometres (Pancheva et al., 2008b).

3 Morphology of the temperature anomalies

The temperature anomalies at 60° N–70° N are shown in Fig. 1a. These anomalies are calculated as the 28-month zonal mean profile (using data from July 2006 to October 2008) subtracted from the daily zonal mean profiles at the respective heights. In this way the mean annual cycle is removed and this data length also includes one full QBO cycle (Zhou et al., 2002; Alexander et al., 2008b). The anomalies are then normalized to the standard deviation at different altitudes to exclude the effect of decreasing density, as displayed in Fig. 1b.

Warm temperature anomalies appear at the beginning of February 2007 and during the entire month of March 2007 as well as in late January, early February and March 2008 centred on 30 km height (Fig. 1a), coinciding with the time of major stratospheric warming and the final stratospheric warming events respectively. These signatures are more pronounced at 65° N–75° N, where the major stratospheric warming from January and February 2008 shows a warm anomaly of as much as 15 K (not shown).

ACPD
9, 14601–14643, 2009

These anomalies reach down to 20 km with the last stratospheric warming in March 2007 reaching down to 15 km before the lower stratosphere settles into its summer condition.

The normalized temperature anomalies indicate a similar pattern but amplitudes are about a factor of 10 smaller than the residuals (Fig. 1b). The cold anomalies are confined to the November–January period extending throughout the altitude range considered here. However, in 2006 and above ∼ 20 km this period is reduced to November–December due to a warm anomaly associated with the stratospheric warming in January 2007. In 2007 the stratospheric warming signature with an amplitude of 0.6 K can be seen embedded in the cold anomaly in February 2007. During the major stratospheric warming in January–February 2008 the warm anomaly reaches 0.9–1.2 K. The manifestation is more dramatic poleward, as expected (e.g. 65° N–75° N, not shown here).

In the Southern Hemisphere the anomaly patterns are somewhat different (Fig. 2). There is annual variability marked by broader warm seasonal anomalies than the cold temperature anomalies. The 2007 winter anomaly appears weaker and shorter in duration than in the winters of 2006 and 2008. This is apparent both in the mapping of the residual and normalized temperature anomalies. A distinct tilt with height is observed (downward phase propagation), which is particularly apparent below 25 km altitude.

4 Planetary wave morphology

4.1 Space-time spectra

At each altitude, COSMIC data are binned into grid cells with latitude width 10° and longitude width 20° and temporal resolution of two days. (Note that this method inherently adds some noise to low s waves.) The two-day zonal mean temperature is removed to form T'. Unlike equatorial wave analysis, it is not necessary to separate the temperature data into symmetrical and anti-symmtrical components (Ern et al., 2009).

ACPD
9, 14601–14643, 2009

Furthermore, the temperature spectra are not red so it is not necessary to divide the results by a background spectrum (Wheeler and Kiladis, 1999; Alexander et al., 2008b; Ern et al., 2008). The analysis period is 96 days, stepped forward in time by 32 days. A Welch window is applied in time to this 96 day data set to minimize spectral leakage. In order to minimize signal suppression, only the middle 32 day interval in each 96 day dataset is retained for further analysis. Henceforth we use the notation E1 to represent any eastward s=1 planetary wave, W1 to represent any westward s=1 planetary wave and so on. When discussing a planetary wave with a particular period, we use the notation e.g. 23DE1 to refer to an s=1 eastward propagating wave with period 23 days.

The wavenumber-frequency s–ω spectra at 60° N–70° N calculated over the interval 1 November 2006 to 4 November 2008 are shown in Fig. 3. The spectra are formed from the average of the eight 96 day intervals during this period, each starting on 1 November, 1 February, 1 May and 1 August for both years, in a similar manner to Speth and Madden (1983). The resultant slight overlapping of spectra is not significant. Averaging the spectra over the eight intervals reduces the noise and uncertainty of the results. Waves with ground based periods of 4 days (the Nyquist period) to 32 days and $|s|<9$ are considered here. When considering ground-based frequencies, as measured by COSMIC and other satellites, the location of a wave in wavenumber-frequency space will not change with altitude under the assumption of a slowly varying background field despite changes in the background wind with altitude (Ern et al., 2008).

The s–ω power spectra for both stationary and travelling waves at 60° N–70° N and 30 km altitude is shown in Fig. 3a. The largest variance and thus largest wave activity is due to waves with $|s|\leq 2$. The spectrum is approximately symmetrical with a near equal amount of variance for the eastward and westward wave components. Most of the planetary waves with $|s|\leq 2$ have ground-based phase speeds c_x of 2.5 m s^{-1} to 20 m s^{-1} and frequencies $\omega<0.15$ cycles per day. The travelling waves are shown in Fig. 3c (calculated from Eq. 7). A significant amount of the westward variance has disappeared, indicating that there are a number of stationary waves with $\omega<0.10$ cycles

ACPD
9, 14601–14643, 2009

per day (i.e. ground-based periods τ>10 days). Most travelling waves are eastward, with ω < 0.10 cycles per day, $|s|\leq 2$ and c_x<20 m s^{-1}.

The s–ω power spectra at 60° S–70° S are slightly different from the Northern Hemisphere spectra (Fig. 3b). When considering the total variance, there are clearly more eastward waves than westward, as expected in the Southern Hemisphere (e.g. Hartmann et al., 1984). The eastward side of the spectra is narrower than in the Northern Hemisphere, with a higher concentration of variance at lower s. Wave speeds and periods are similar to the Northern Hemisphere. After removal of the stationary waves, essentially only eastward travelling waves remain (Fig. 3d).

Spectra at other altitudes are also studied. As an example, the results from 15 km are shown in Fig. 4. A close inspection of the Northern Hemisphere (60° N–70° N) variance distribution of all wave components in Fig. 4a reveals waves with a somewhat lower c_x and less symmetry at 15 km than 30 km. Removal of the stationary wave component results in the complete absence of westward propagating waves with ω>0.07 cycles per day and c_x<−10 m s^{-1} (Fig. 4c). The 15 km spectra are not evenly distributed between eastward and westward components: there are more eastward waves with higher c_x and larger ω than in westward direction.

In contrast, the Southern Hemisphere s–ω power spectra at 15 km are nearly identical in shape to those at 30 km. The spectra at both altitudes show a preference for eastward waves, which are primarily travelling (Fig. 4d), whereas the westward components are almost entirely due to stationary waves. Larger travelling wave variance at s=2 and ω~0.15 cycles per day is noticed at 15 km than at 30 km.

4.2 Seasonal wave activity

Zonal wavenumbers of $s\geq 4$ are indicative of tropospheric baroclinic waves (Randel, 1987; Watanabe et al., 2008), thus we consider only $s\leq 3$ here. Furthermore, the s–ω spectra in Fig. 3 show that nearly all of the power is associated with low $|s|$ waves. Hövmoller diagrams are reconstructed using these wave filtered regions (not shown) to check that the filtering gives meaningful results when compared to the original binned

ACPD
9, 14601–14643, 2009

temperature data. While results obtained for the $|s|$=3 waves are physically reasonable, the total amplitudes are generally <2 K, making them insignificant compared to the $|s|$=1 and $|s|$=2 waves, so they are not considered further.

The travelling planetary wave amplitudes $A_{s,j}$ (from Eq. 8) for the $|s|\leq 2$ waves, being the sum of the discrete periods τ_j are shown in Fig. 5 for the period September 2006–November 2008. As expected, large planetary wave activity is present during winter, while it is almost completely absent during summer when the background wind speeds $\overline{u}$<0 m s^{-1}. Intermittent bursts of planetary wave activity are noted during both winters, most of which are related to the SSWs to be discussed below. Amplitudes of westward propagating waves are generally less than those of the eastward waves. The time of the final warming of the winter polar stratosphere varies each year because it is dependent upon pre-existing conditions in the stratosphere (Waugh and Rong, 2002). The final warming is initiated by transient Rossby waves propagating upward from the troposphere which affect the Arctic stratosphere and troposphere simultaneously (Black et al., 2006), hence the near constant decrease in zonal wind speeds with altitude evident during the final spring warmings in Fig. 5.

The planetary wave amplitudes at 60° S–70° S are shown in Fig. 6. In the Southern Hemisphere, the eastward waves have much larger amplitudes than the westward waves. The amplitudes of E1 and E2 are directly related to the background zonal wind. Note in particular the downward propagation of eastward winds during winter and spring and the associated downward propagation of enhanced planetary wave amplitude (especially visible during 2007). Eastward waves cease to exist when the background wind speed is ∼0 m s^{-1}. Compared to the Northern Hemisphere, relatively small amounts of westward wave activity are seen during both springs.

4.3 Temporal variability of the dominant wave periods

The time series for the discrete s, extracted via Eq. (8), are used to calculate wavelet spectra in order to study the temporal variability of the dominant travelling wave periods τ (see Sect. 2.3 above). A Morlet wavelet is used as the orthonormal wavelet because

ACPD
9, 14601–14643, 2009

the temperature perturbation data are amplitude-modulated sine waves. Specifically, the Morelet wavelet $\psi_0(t)$ is a plane-modulated Gaussian function:

$$\psi_o(t) = \pi^{1/4} e^{6it} e^{-t^2/2}. \quad (9)$$

Amplitude and phase information can be extracted from the one dimensional time series because the Morelet wavelet is complex (Torrence and Compo, 1998). Data are zero padded to remove end wraparound effects prior to calculating the wavelet transform. The wavelet power spectrum at 30 km and 60° N–70° N for travelling waves with periods τ between 4 days and 32 days are shown in Fig. 7 for each of E1, W1, E2 and W2. The strongest wintertime E1 have τ~16 days and τ>20 days during 2007 and τ=12–16 days during 2008. The variance of the W1 waves is smaller and the strongest W1 have τ between 10 days and about 24 days during both winters. The E2 and W2 waves show similar levels of activity. A strong 16–20 day E2 wave peaks during early February 2008, close in time to a lot of W2 activity with a variety of periods from 8 days upwards. When these travelling wave plots are compared to the wavelet analysis of the stationary and travelling components combined (not shown), the results are similar for most of the short period activity, but there is less variance at longer periods, indicative of stationary waves.

The 60° S–70° S and 30 km altitude travelling planetary wave power spectra are shown in Fig. 8. Large interannual variability in planetary wave activity between each of the three springs is evident in the Southern Hemisphere. The dominant E1 have τ~12–23 days. The substantially weaker W1 has largest variance around 16–23 days. The E2 generally have shorter periods than the $|s|$=1 waves, often about 8–12 days. In comparison, the very weak W2 are inclined to have τ>16 days. A large amount of wave activity is observed during November and December 2006. These planetary waves were studied in detail by Shepherd and Tsuda (2008) and this analysis agrees with the results presented in that paper. There is correspondingly little planetary wave activity in November and December 2007, suggestive of the known inter-annual variability of the Southern Hemisphere stratosphere (Shiotani et al., 1993). While a 5 day

ACPD
9, 14601–14643, 2009

wave is fitted to the data in Eq. (8), there is no variance significant at the 95% level for the $|s| \leq 2$ components in either hemisphere.

5 Planetary wave activity during the Arctic sudden stratospheric warmings

5.1 Background dynamical fields

Several sudden stratospheric warmings (SSWs) occurred during the Arctic winters of 2006/2007 and 2007/2008. Planetary wave activity preceding and during these warmings is studied in detail using COSMIC data. Firstly, the UKMO background zonal mean temperature and zonal mean zonal wind in 2006/2007 between 45° N and 85° N is displayed in Fig. 9a on the 10 hPa surface. We display UKMO data because the SSW definition involves 10 hPa dynamical fields (Labitzke and Naujokat, 2000), although a check reveals COSMIC temperatures at 30–32 km to be essentially the same (not shown). A reversal in meridional temperature gradient occurs in early January, early February and late February/early March. Only the last of these is also associated with a complete reversal in direction of the zonal mean zonal wind at 10 hPa to westward and as such is the only major SSW. The background fields between 1000 hPa and 1 hPa at 60° N–70° N are shown in Fig. 9b. An increase in temperature is noted during the late February major SSW, while there is not a clear change in temperature during the minor SSWs from this plot.

Similarly, the 45° N–85° N background fields during the winter of 2007/2008 at 10 hPa are shown in Fig. 9c. Four SSWs are evident: in late January, early February, mid February and late February. Except for the mid-February SSW, the meridional temperature gradient reversals are larger than those during the previous winter. The late February SSW is classified as major as it is also accompanied by westward winds. During this SSW, zonal mean zonal winds peaked at between -20 m s^{-1} and -30 m s^{-1},

ACPD
9, 14601–14643, 2009

before returning to 10 m s^{-1} to 20 m s^{-1} in early March. Clear increases in temperature occur during all of the SSWs (Fig. 9d).

The temperature perturbations from the zonal mean observed by COSMIC in the latitude bin 60° N–70° N are calculated over two day intervals (independently) and are shown as Hövmoller diagrams in Fig. 10a for the winter of 2006/2007 and Fig. 10d for 2007/2008. Higher temperatures at 180° E occur during both winters, as a result of the zonally asymmetric structure associated with the stationary s=1 Aleutian High and corresponding low over Scandinavia (Pawson and Kubitz, 1996). Eastward propagating waves, extracted using Eq. (8), are clearly visible throughout both winters (Fig. 10b and e). Westward propagating waves are strongest during February 2007 (Fig. 10c) and from late January 2008 onwards (Fig. 10f). Note the presence of the 0 m s^{-1} zonal mean zonal wind in late February 2007 in Fig. 10a and late February 2008 in Fig. 10d. Figure 10b and e show a large amount of E1 and E2 activity, with total amplitudes often around 20 K. Westward waves are generally of lower amplitude (mostly <10 K), with W1 dominating. Shorter E1 and W1 periods on the order of 10–14 days are apparent during January and February 2008, as noted in the wavelet analysis of Fig. 7.

5.2 Latitudinal distribution of planetary waves

The amplitudes of the dominant planetary waves at 30 km between 20° N and 80° N during the 2006/2007 winter are shown in Fig. 11. Wave amplification occurs over a wide latitude band. The SPW1 has its largest amplitude during the first minor SSW (Fig. 11a), suggesting it plays an important role in reversing the meridional temperature gradient (Fig. 9a). The 23DE1 planetary wave has local maxima in mid-December, early February and late February (prior to the major SSW), while the 16DE1 has a single maximum during January. A distinct change in the latitude of maximum amplitude of the 16DE2 and 23DE2 occurs at the start of January, co-inciding with the first minor SSW. Before then, these waves are centred at 40° N, while afterwards the centre is at 50° N. The SPW2 also shows a shift poleward during early January. It is the only

ACPD
9, 14601–14643, 2009

planetary wave to reform signficantly after the late February major SSW. The eastward waves likely pre-condition the stratosphere (Labitzke, 1981; Krüger et al., 2005) not only for the major SSW in late February but are also likely to do so for the first minor SSW in early January. The largest amplitude westward waves are the 23DW2 and the 23DW1. Both the 23DW2 and 23DW1 have a broad maximum throughout February (the 23DW2 centred on 50° N and the 23DW1 centred on 60° N) and both decay rapidly in amplitude as the major SSW occurs. The 23DW1 has a number of other increases in activity earlier in the winter, primarily before and during the first minor SSW.

The equivalent dominant planetary waves during winter 2007/2008 are shown in Fig. 12. Note that the 12DE1 is displayed instead of the 23DW2 because the amplitude of the latter is small except for briefly in early February (see also Fig. 13h below). Large SPW2 amplitude is observed throughout February, centred on 60° N, and decays with the onset of the major SSW in late February. The 23DW1 also decays immediately prior to the major SSW, yet reforms with greater amplitude upon its cessation. Decreases in planetary wave amplitudes are also observed during the minor SSW of late January, during which time the 12DE1, 16DE1 and 16DE2 decay before reforming rapidly in early February. The planetary wave amplitudes of the 23DE1 and 23DE2 components are larger throughout January but do not regain their previous intensity after the minor SSW. The 16DE1 and 16DE2 appear responsible for the minor SSW of early February because of a short burst of enhanced activity during this time.

5.3 Planetary waves at 60° N–70° N

The amplitudes of specific period planetary waves at 30 km reconstructed from the data during the 2006/2007 winter are shown in Fig. 13a–d for 60° N–70° N. These have been smoothed by a five-day running mean. Similar planetary wave activity is also observed in the neighbouring latitude bin of 50° N–60° N (not shown, but apparent from Fig. 11). We focus on 60° N–70° N because it is inside the SSW definition latitude range (Labitzke and Naujokat, 2000). The τ=5 day waves are not shown here because their amplitudes are consistently <1 K.

ACPD
9, 14601–14643, 2009

The SPW1 wave has a maximum amplitude of 15 K in early January 2007 before steadily decreasing for the remainder of the winter (Fig. 13a). The 23DE1 planetary wave has two maxima: the first in mid-December and the second in late February, while the 16DE1 has a single maximum during January. E2 wave amplitudes are also enhanced during February, with broad maxima for all of the 12DE2, 16DE2 and 23DE2 components (Fig. 13c), but the SPW2 varies little in amplitude throughout the winter. Amplitudes of the W1 are generally less than E1. A doubling in amplitude of the 16DW1 occurs in mid-January and in late February/early March, whereas the 23DW1 amplitudes behave in an opposite way. A strong increase in 23DW2 activity is co-incident with the early February minor warming.

The amplitudes of specific period planetary waves during the 2007/2008 winter are shown in Fig. 13e–h. The behaviour of the SPW1 during 2007/2008 is similar to the preceding winter, with a maximum in January and a steady decline thereafter. 12DE1 and 16DE1 waves are largest from early January until mid-February, after which the major SSW occurs. The 23DE1 is amplified from early to mid-January, prior to the first minor SSW. The largest amplitude E2 wave during winter is the 16DE2, except during the first minor SSW in late January, when a 23DE2 wave dominates. The SPW2 exhibits different behaviour during 2007/2008 when compared to the previous winter. It grows in amplitude from ∼2 K in mid-January to 5 K in early February, co-incident with the second minor warming. There are large variations in the westward wave amplitudes during this winter. Local maxima in the 16DW1, 23DW1 and 23DW2 occur from late January to early February. During the major SSW, increases in amplitude of the 23DW1, and the 16DW2 are most prominent.

6 Discussion

Properites of the dominant planetary waves present during the 2007 and 2008 SSWs are summarised in Tables 1 and 2 respectively. Anomalously large E1 activity from waves with various periods preconditions the stratospheric circulation prior to most of

ACPD
9, 14601–14643, 2009

the SSWs, as expected climatologically (Labitzke, 1981; Limpasuvan et al., 2004) and observed e.g. during the recent Northern Hemisphere winters of 2003/2004 (Pancheva et al., 2008b) and 2005/2006 (Hoffmann et al., 2007). Large amplitudes of the ground-based westward propagating waves occur immediately prior to the large decrease in zonal mean zonal wind, with maximum westward winds often occurring after cessation of large eastward wave activity. For all of the planetary waves recorded here, $c_x < \overline{u}$, so all of these intrinsically westward propagating waves decelerate the eastward flow (Holton, 2004).

During the 2007/2008 winter, 12DE1 and 16DE1 waves are superimposed upon an SPW1 at 30 km (Figs. 10, 12 and 13). The amplitudes of the 12DE1 and 16DE1 drop sharply immediately prior to the onset of the major SSW in late February 2008 (Fig. 13e), consistent with the general development of an s=1 major warming (Labitzke, 1977; Krüger et al., 2005). Large SPW2 and an increase in 16DW2 occur during the major SSW (Fig. 13g and h), although the peak SPW2 amplitude occurs in early February.

Unlike the winter of 2007/2008, during 2006/2007 the two largest amplitude E1 waves (in this case the 16DE1 and 23DE1) have their largest amplitudes at the time when the other wave's amplitude is relatively small. Nevertheless, both of these waves decay rapidly in amplitude from late February 2007 (Fig. 13a) at the onset of the major SSW, although not as dramatically as the decay in 2008. The s=2 components are <3 K throughout the winter of 2006/2007. Compared to 2007/2008, the 2006/2007 SPW2 activity is much weaker throughout all of winter.

The periods of the travelling planetary waves which account for nearly all of the total travelling wave activity are consistent with previous observations of SSWs. The 16DE1 wave was observed in the horizontal wind during the 2003/2004 SSW in the stratosphere and MLT region, with amplitude amplification prior to onset (Pancheva et al., 2008b), consistent with the 2008 results in the low to mid stratosphere presented here. Palo et al. (2005) demonstrated the presence of a 10DE1 superimposed upon an SPW1 at 30 km prior to the major Antarctic SSW of 2002, while Chshyolkova

ACPD
9, 14601–14643, 2009

et al. (2005, 2006) found s=1 with periods of 20–30 days throughout the entire Arctic middle atmosphere during winters 2000–2002. A westward 16 day wave was observed throughout the stratosphere and mesosphere during the winter of 2003/2004 (Pancheva et al., 2008b), amongst other waves of periods 5–6 days, 10–12 days, 15–17 days and 24 days (Pancheva et al., 2009b).

Stationary planetary waves in both winters are also related to the warmings and their amplification appears to play a role in causing some of the SSWs (Figs. 11 and 12). The SPW1 during 2006/2007 has its largest amplitude during the first minor warming, however, the peak amplitude during 2007/2008 is not co-incident with any warming. The SPW2 exhibits large variability between winters. During both winters, its largest amplification occurs prior to the major SSWs and its amplitude reduces significantly during the major SSWs. During 2006/2007, the SPW2 reforms immediately after the SSW.

This analysis during the 2006/2007 and 2007/2008 winters illustrates the importance of E1 waves in preconditioning the Northern Hemisphere stratosphere prior to the SSWs. However, the amplitudes and periods of these E1 waves vary between years (Figs. 7a, 13a and e). Southern Hemisphere planetary wave activity is dominated by the E1 and E2 waves which have largest amplitude during spring, co-incident in time with the largest zonal wind speeds. Enhanced wave amplitudes descend in time in concert with the descending zonal wind structure as the vortex decays during late spring. The presence of E2 waves with periods around 10 days at 60° S was noted at 10 hPa (close to 30 km geometric altitude) in spring by Shiotani et al. (1990). E2 waves of similar periods are also observed in the COSMIC data in each of the three springs (Fig. 8c).

The COSMIC temperature s–ω power spectra of Figs. 3 and 4 agree with previous observational and model analyses at similar altitudes in the mid-latitude Northern Hemisphere which used geopotential height or geostrophic wind (Fraedrich and Böttger, 1978; Watanabe et al., 2008). Hayashi and Golder (1977) illustrated the latitude-height differences of the geopotential, zonal, temperature and vertical pressure

ACPD
9, 14601–14643, 2009

velocity components of planetary wave power spectra. The COSMIC results also agree with the latitudinal structure of the temperature components presented by Hayashi and Golder (1977).

To investigate the COSMIC spectra further, UKMO assimilated dynamical data on the 100 hPa and 10 hPa isobars are studied (close to the 15 km and 30 km presented here). At 60° N–70° N, the resultant temperature s–ω spectra and the Hövmoller diagrams are nearly identical to Figs. 3 and 4 (not shown). Next, the UKMO geopotential heights are considered. In this case, at 10 hPa and 100 hPa, a significant amount of the E1 planetary waves are stationary, while E2 are mainly travelling. Larger variances existed for the travelling W1 and W2 than for eastward components. These results are consistent with those of Speth and Madden (1983). We also note here that the Hövmoller diagrams of the geopotential heights exhibit some differences to the temperature Hövmoller diagrams (not shown). A full dynamical analysis of planetary waves during 2007 and 2008 is possible with assimilated data such as UKMO, although it is beyond the scope of the present study.

7 Conclusions

Temperature data from the COSMIC GPS-RO satellite constellation are used to probe the large scale structure and dynamics of the mid to high latitude stratosphere of both hemispheres from September 2006 until November 2008 via a study of planetary wave activity. During the boreal winters of 2006/2007 and 2007/2008, several sudden stratospheric warmings (SSWs) occur, including a major one during each winter.

An overview of planetary wave activity during the period studied is presented using space-time spectral analysis. This shows that there are more eastward propagating waves than westward at 30 km and 60° N–70° N, with ω<0.10 cycles per day, $|s|\leq 2$ and c_x<20 m s^{-1}. Large amounts of stationary wave activity are also present in the Northern Hemisphere. At 60° S–70° S, most of the travelling wave variance is associated with eastward propagating waves, with very little westward activity other than some $s=-1$.

ACPD
9, 14601–14643, 2009

The shape of the wave spectra change with altitude, due to increasingly strong winds higher in the stratosphere. Individual planetary waves are then extracted via a linear least squares fitting routine and their vertical structure and periods examined. Most of the large Northern Hemisphere wave activity is associated with the winter SSWs, while the largest amplitude waves in the Southern Hemisphere occurred in spring, coincident in time with the descent of the strongest zonal wind speeds during the vortex decay phase.

Planetary wave activity during the SSWs is due largely to travelling waves with $|s| \leq 2$ having periods of 12, 16 and 23 days and to stationary waves with $s=1$ and $s=2$. The SPW2 is amplified prior to both major SSWs and decays rapidly during the actual events. Amplitudes of the 23DW2, 23DW1, 23DE1 decrease significantly with onset of the major SSWs during February 2007. For the major SSW in the following February, all planetary waves decay significantly, with only the 23DW1 reforming after SSW cessation.

Acknowledgements. We would like to thank T. Tsuda, Y. Kawatani and A. Klekociuk for valuable discussions and advice throughout the course of this research. This research was conducted for project 3140 of the Australian Antarctic programme.

References

Alexander, S. P., Tsuda, T., and Kawatani, Y.: COSMIC GPS Observations of Northern Hemisphere winter stratospheric gravity waves and comparisons with an atmospheric general circulation model, Geophys. Res. Lett., 35, L10808, doi:10.1029/2008GL033174, 2008a. 14605

Alexander, S. P., Tsuda, T., Kawatani, Y., and Takahashi, M.: Global distribution of atmospheric waves in the equatorial upper troposphere and lower stratosphere: COSMIC observations of wave mean flow interactions, J. Geophys. Res., 113, D24115, doi:10.1029/2008JD010039, 2008b. 14604, 14605, 14606, 14609, 14611

Alexander, S. P., Klekociuk, A. R., and Tsuda, T.: Gravity wave and orographic wave activity

observed around the Antarctic and Arctic stratospheric vortices by the COSMIC GPS-RO satellite constellation, J. Geophys. Res., doi:10.1029/2009JD011851, in press, 2009. 14604

Andrews, D. G., Holton, J. R., and Leovy, C. B.: Middle Atmosphere Dynamics, Academic Press, 1987. 14602, 14603

Anthes, R. A., Bernhardt, P. A., Chen, Y., Cucurull, L., Dymond, K. F., Ector, D., Healy, S. B., Ho, S. P., Hunt, D. C., Kuo, Y. H., Liu, H., Manning, K., McCormick, C., Meehan, T. K., Randel, W. J., Rocken, C., Schreiner, W. S., Sokolovskiy, S. V., Syndergaard, S., Thompson, D. C., Trenberth, K. E., Wee, T. K., Yen, N. L., and Zeng, Z.: The COSMIC/FORMSAT-3 Mission Early Results, Bull. Amer. Meteor. Soc., 89, 313–333, doi:10.1175/BAMS-89-3-313, 2008. 14604

Black, R. X., McDaniel, B. A., and Robinson, W. A.: Stratosphere-troposphere coupling during spring onset, J. Climate, 19, 4891–4901, 2006. 14613

Chshyolkova, T., Manson, A. H., Meek, C. E., Avery, S. K., Thorsen, D., MacDougall, J. W., Hocking, W., Murayama, Y., and Igarashi, K.: Planetary wave coupling in the middle atmosphere (20–90 km): A CUJO study involving TOMS, MetO and MF radar data, Ann. Geophys., 23, 1103–1121, 2005. 14602, 14619

Chshyolkova, T., Manson, A. H., Meek, C. E., Avery, S. K., Thorsen, D., MacDougall, J. W., Hocking, W., Murayama, Y., and Igarashi, K.: Planetary wave coupling processes in the middle atmosphere (30–90km): A study involving MetO and MFR data, J. Atmos. Sol. Terr. Phys., 68, 358–368, 2006. 14603, 14604, 14620

Dowdy, A. J., Vincent, R. A., Tsutsumi, M., Igarashi, K., Murayama, Y., Singer, W., Murphy, D. J., and Riggin, D. M.: Polar mesosphere and lower thermosphere dynamics: 2. Response to sudden stratospheric warmings, J. Geophys. Res., 112, D17105, doi:10.1029/2006JD008127, 2007. 14604

Duck, T. J., Whiteway, J. A., and Carswell, A. I.: Lidar observations of gravity wave activity and Arctic stratospheric vortex core warming, Geophys. Res. Lett., 25, 2813–2816, 1998. 14604

Dunkerton, T. J. and Butchart, N.: Propagation and selective transmission of internal gravity waves in a sudden warming, J. Atmos. Sci., 41, 1443–1460, 1984. 14604

Ern, M., Preusse, P., Krebsbach, M., Mlynczak, M. G., and Russell III, J. M.: Equatorial wave analysis from SABER and ECMWF temperatures, Atmos. Chem. Phys., 8, 845–869, 2008. 14606, 14611

Ern, M., Lehmann, C., Kaufmann, M., and Riese, M.: Spectral wave analysis at the mesopause from SCIAMACHY airglow data compared to SABER temperature spectra, Ann. Geophys.,

27, 407–416, 2009. 14606, 14610
Fraedrich, K. and Böttger, H.: A wavenumber-frequency analysis of the 500 mb geopotential at 50° N, J. Atmos. Sci., 35, 745–750, 1978. 14620
Garcia, R. R., Lieberman, R., Russell III, J. M., and Mlynczak, M. G.: Large scale waves in the mesosphere and lower thermosphere observed by SABER, J. Atmos. Sci., 62, 4384–4399, 2005. 14606
Hartmann, S. L., Mechoso, C. R., and Yamazaki, K.: Observations of wave mean flow interaction in the Southern Hemisphere, J. Atmos. Sci., 41, 351–162, 1984. 14602, 14603, 14612
Hayashi, H., Furumoto, J., Lin, X., Tsuda, T., Shoji, Y., Aoyama, Y., and Maruyama, Y.: Validation of refractivity profiles retrieved from FORMOSAT-3/COSMIC radio occultation soundings: Preliminary results of statistical comparisons utilizing balloon-borne observations, Terr. Atmos. Ocean. Sci., 20, 51–58, doi:10.3319/TAO.2008.01.21.01(F3C), 2009. 14605
Hayashi, Y.: A generalized method of resolving disturbances into progressive and retrogressive waves by space Fourier and time cross-spectral analysis, J. Met. Soc. Japan, 49, 125–128, 1971. 14606, 14607
Hayashi, Y.: On the coherence between progressive and retrogressive waves and a partition of space-time power spectra into standing and traveling parts, J. Appl. Meteorol., 16, 368–373, 1977. 14607
Hayashi, Y.: Space-time spectral analysis and its applications to atmospheric waves, J. Met. Soc. Japan, 60, 156–171, 1982. 14607
Hayashi, Y. and Golder, D. G.: Space-time spectral analysis of mid-latitude disturbances appearing in a GFDL general circulation model, J. Atmos. Sci., 34, 237–262, 1977. 14620, 14621
Hirooka, T.: Normal mode Rossby waves as revealed by UARS/ISAMS observations, J. Atmos. Sci., 57, 1277–1285, 2000. 14603
Hirooka, T. and Hirota, I.: Normal mode Rossby waves observed in the upper stratosphere. Part II: Second antisymmetric and symmetric modes of zonal wavenumbers 1 and 2, J. Atmos. Sci., 42, 536–548, 1985. 14606
Hirota, I. and Hirooka, T.: Normal mode Rossby waves observed in the upper stratosphere. Part I: First symmetric modes of zonal wavenumbers 1 and 2, J. Atmos. Sci., 41, 1253–1267, 1984. 14603, 14606
Hoffmann, P., Singer, W., Keuer, D., Hocking, W. K., Kunze, M., and Murayama, Y.: Latitudinal and longitudinal variability of mesospheric winds and temperatures during stratospheric

warming events, J. Atmos. Sol. Terr. Phys., 69, 2355–2366, 2007. 14603, 14604, 14619
Holton, J. R.: An introduction to dynamic meteorology, Academic Press, 2004. 14603, 14619
Kawatani, Y., Takahashi, M., Sato, K., Alexander, S. P., and Tsuda, T.: Global distribution of atmospheric waves in the equatorial upper troposphere and lower stratosphere: AGCM simulation of sources and propagation, J. Geophys. Res., 114, D01102, doi: 10.1029/2008JD010374, 2009. 14605
Krüger, K., Naujokat, B., and Labitzke, K.: The unusual midwinter warming in the Southern Hemisphere stratosphere 2002: A comparison to Northern Hemisphere phenomena, J. Atmos. Sci., 62, 603–613, 2005. 14603, 14604, 14617, 14619
Kursinski, E. R., Hajj, G. A., Schofield, J. T., Linfield, R. P., and Hardy, K. R.: Observing Earth's atmosphere with radio occultation measurements using the Global Positioning System, J. Geophys. Res., 102, 23429–23465, 1997. 14604, 14605
Labitzke, K.: Interannual variability of the winter stratosphere in the Northern Hemisphere, Mon. Weather Rev., 105, 762–770, 1977. 14619
Labitzke, K.: The amplification of height wave 1 in January 1979: A characteristic precondition for the major warming in February, Mon. Weather Rev., 109, 983–989, 1981. 14617, 14619
Labitzke, K. and Naujokat, B.: The lower Arctic stratosphere in winter since 1952, SPARC Newsl., 11–14, 2000. 14603, 14615, 14617
Leovy, C. B. and Webster, P. J.: Stratospheric long waves: Comparison of thermal structure in the Northern and Southern Hemispheres, J. Atmos. Sci., 33, 1624–1638, 1976. 14603
Limpasuvan, V., Thompson, D. W. J., and Hartmann, D. L.: The life cycle of the Northern Hemisphere sudden stratospheric warmings, J. Climate, 17, 2584–2596, 2004. 14619
Liu, H. L. and Roble, R. G.: A study of a self-generated stratospheric sudden warming and its mesospheric-lower thermospheric impacts using the coupled TIME-GCM/CCM3, J. Geophys. Res., 107, 4695, doi:10.1029/2002JD001533, 2002. 14603
Liu, H. L. and Roble, R. G.: Dynamical coupling of the stratosphere and mesosphere in the 2002 Southern Hemisphere major stratospheric sudden warming, Geophys. Res. Lett., 32, L13804, doi:10.1029/2005GL022939, 2005. 14603, 14604
Manney, G. L., Krüger, K., Sabutis, J. L., Sena, S. A., and Pawson, S.: The remarkable 2003–2004 winter and other recent warm winters in the Arctic stratosphere since the late 1990s, J. Geophys. Res., 110, D04107, doi:10.1029/2004JD005367, 2005. 14603
Manney, G. L., Krüger, K., Pawson, S., Minschwaner, K., Schwartz, M. J., Daffer, W. H., Livesey, N. J., Mlynczak, M. G., Remsberg, E. E., Russell III, J. M., and Waters, J. W.: The evolution

of the stratopause during the 2006 major warming: Satellite data and assimilated meteorological analyses, J. Geophys. Res., 113, D11115, doi:10.1029/2007JD009097, 2008. 14604
Matsuno, T.: A dynamical model of the stratospheric sudden warming, J. Atmos. Sci., 28, 1479–1494, 1971. 14603
Mechoso, C. R. and Hartmann, D. L.: An observational study of traveling planetary waves in the Southern Hemisphere, J. Atmos. Sci., 39, 1921–1935, 1982. 14603, 14606
Murphy, D. J., French, W. J. R., and Vincent, R. A.: Long period planetary waves in the mesosphere and lower thermosphere above Davis, Antarctica, J. Atmos. Sol. Terr. Phys., 69, 2118–2138, 2007. 14604
Newman, P. A. and Nash, E. R.: The unusual Southern Hemisphere stratosphere winter of 2002, J. Atmos. Sci., 62, 614–628, 2005. 14603
Palo, S. E., Forbes, J. M., Zhang, X., Russell III, J. M., Mertens, C. J., Mlynczak, M. G., Burns, G. B., Espy, P. J., and Kawahara, T. D.: Planetary wave coupling from the stratosphere to the thermosphere during the 2002 Southern Hemisphere pre-stratwarm period, Geophys. Res. Lett., 32, L23809, doi:10.1029/2005GL024298, 2005. 14603, 14619
Palo, S. E., Forbes, J. M., Zhang, X., Russell III, J. M., and Mlynczak, M. G.: An eastward propagating two-day wave: Evidence for nonlinear planetary wave and tidal coupling in the mesosphere and lower thermosphere, Geophys. Res. Lett., 34, L07807, doi:10.1029/2006GL027728, 2007. 14606
Pancheva, D., Mukhtarov, P., Mitchell, N. J., Andonov, B., Merzlyakov, E., Singer, W., Murayama, Y., Kawamura, S., Xiong, J., Wan, W., Hocking, W., Fritts, D., Riggin, D., C., M., and Manson, A.: Latitudinal wave coupling of the stratosphere and mesosphere during the major stratospheric warming in 2003/2004, Ann. Geophys., 26, 467–483, 2008a. 14603
Pancheva, D., Mukhtarov, P., Mitchell, N. J., Merzlyakov, E., Smith, A. K., Andonov, B., Singer, W., Hocking, W., Meek, C., Manson, A., and Murayama, Y.: Planetary waves in coupling the stratosphere and mesosphere during the major stratospheric warming in 2003/2004, J. Geophys. Res., 113, D12105, doi:10.1029/2007JD009011, 2008b. 14604, 14608, 14609, 14619, 14620
Pancheva, D., Mukhtarov, P., Andonov, B., Mitchell, N. J., and Forbes, J. M.: Planetary waves observed by TIMED/SABER in coupling the stratosphere-mesosphere-lower thermosphere during the winter of 2003/2004: Part 2 – Altitude and latitude planetary wave structure, J. Atmos. Sol. Terr. Phys., 71, 75–87, 2009a. 14603, 14609
Pancheva, D., Mukhtarov, P., Andonov, B., Mitchell, N. J., and Forbes, J. M.: Planetary waves

ACPD
9, 14601–14643, 2009

observed by TIMED/SABER in coupling the stratosphere-mesosphere-lower thermosphere during the winter of 2003/2004: Part 1 – Comparison with the UKMO temperature results, J. Atmos. Sol. Terr. Phys., 71, 61–74, 2009b. 14620

Pancheva, D. V., Mukhtarov, P. J., and Andonov, B. A.: Zonally symmetric oscillations in the Northern Hemisphere stratosphere during the winter of 2003–2004, Geophys. Res. Lett., 34, L04807, doi:10.1029/2006GL028666, 2007. 14609

Pawson, S. and Kubitz, T.: Climatology of planetary waves in the northern stratosphere, J. Geophys. Res., 101, 16987–16996, 1996. 14616

Randel, W. J.: A study of planetary waves in the southern winter troposphere and stratosphere. Part I: Wave stucture and vertical propagation, J. Atmos. Sci., 44, 917–935, 1987. 14603, 14612

Randel, W. J. and Wu, F.: Kelvin wave variability near the equatorial tropopause observed in GPS radio occultation measurements, J. Geophys. Res., 110, D03102, doi:10.1029/2004JD005006, 2005. 14606

Ratnam, M. V., Tsuda, T., Jacbi, C., and Aoyama, Y.: Enhancement of gravity wave activity observed during a major Southern Hemisphere stratospheric warming by CHAMP/GPS measurements, Geophys. Res. Lett., 31, L16101, doi:10.1029/2004GL019789, 2004. 14604

Schreiner, W., Rocken, C., Sokolovskiy, S., Syndergaard, S., and Hunt, D.: Estimates of the precision of GPS radio occultations from the COSMIC/FORMOSAT-3 mission, Geophys. Res. Lett., 34, L04808, doi:10.1029/2006GL027557, 2007. 14605

Shepherd, M. G. and Tsuda, T.: Large scale planetary disturbances in stratospheric temperature at high latitudes in the southern summer hemisphere, Atmos. Chem. Phys., 8, 7557–7570, 2008. 14604, 14608, 14609, 14614

Shepherd, M. G., Wu, D. L., Fedulina, I. N., Gurubaran, S., Russell, J. M., Mlynczak, M. G., and Shepherd, G. G.: Stratospheric warming effects on the tropical mesospheric temperature field, J. Atmos. Sol. Terr. Phys., 69, 2309–2337, 2007. 14604

Shiotani, M., Kuroi, K., and Hirota, I.: Eastward travelling waves in the southern hemisphere stratosphere during the spring of 1983, Q. J. Roy. Meteorol. Soc., 116, 913–927, 1990. 14602, 14620

Shiotani, M., Shimoda, N., and Hirota, I.: Interannual variability of the stratospheric circulation in the southern hemisphere, Q. J. Roy. Meteorol. Soc., 119, 531–546, 1993. 14614

Speth, P. and Madden, R. A.: Space-time spectral analyses of Northern Hemisphere geopotential heights, J. Atmos. Sci., 40, 1086–1100, 1983. 14606, 14611, 14621

Torrence, C. and Compo, G. P.: A practical guide to wavelet analysis, Bull. Amer. Meteor. Soc., 79, 61–78, 1998. 14614, 14637

Tsuda, T., Nishida, M., Rocken, C., and Ware, R. H.: A global morphology of gravity wave activity in the stratosphere revealed by the GPS occultation data (GPS/MET), J. Geophys. Res., 105, 7257–7273, 2000. 14604

Watanabe, S., Kawatani, Y., Tomikawa, Y., Miyazaki, K., Takahashi, M., and Sato, K.: General aspects of a T213L256 middle atmosphere general circulation model, J. Geophys. Res., 113, D12110, doi:10.1029/2008JD010026, 2008. 14606, 14612, 14620

Waugh, D. W. and Rong, P. P.: Interannual variability in the decay of lower stratospheric Arctic vortices, J. Met. Soc. Japan, 80, 997–1012, 2002. 14613

Wheeler, M. and Kiladis, G. N.: Convectively Coupled Equatorial Waves: Analysis of Clouds and Temperature in the Wavenumber-Frequency Domain, J. Atmos. Sci., 56, 374–399, 1999. 14606, 14611

Zhou, S., Miller, A. J., Wang, J., and Angell, J. K.: Downward propagating temperature anomalies in the preconditioned polar stratosphere, J. Climate, 15, 781–792, 2002. 14609

Table 1. Properties of major planetary waves at 30 km and 60° N–70° N during the 2007 SSWs. A co-incident SSW is one that occurs simultaneously in time with the maximum planetary wave amplitude, but does not necessarily imply causality.

Co-incident SSW	Time of Peak Amplitude	Wave τ and s	c_x (m s^{-1})	Amplitude (K)
–	mid December	23DE1	9	8.0
Minor	early January	SPW1	0	15.0
–	late January	16DE1	12	8.5
Minor	early February	23DW2	–4	2.0
–	mid February	SPW2	0	3.0
Major	late February	23DE1	9	5.0
Major	late February	16DW1	–16	2.5

ACPD
9, 14601–14643, 2009

Table 2. Properties of major planetary waves at 30 km and 60° N–70° N during the 2008 SSWs.

Co-incident SSW	Time of Peak Amplitude	Wave τ and s	c_x (m s^{-1})	Amplitude (K)
Minor	early January	23DE1	9	4.0
–	January	SPW1	0	15.0
–	mid January	12DE1	16	7.0
Minor	late January	23DE2	4	3.0
Minor	early February	SPW2	0	5.0
Minor	early February	16DE1	12	8.0
Minor	early February	16DE2	6	3.0
Minor	early February	16DW1	–12	4.0
Minor	early February	23DW1	–9	5.0
Minor	early February	23DW2	–4	3.0
Major	early March	23DW1	–9	5.0
Major	early March	16DW2	–6	2.0

ACPD
9, 14601–14643, 2009

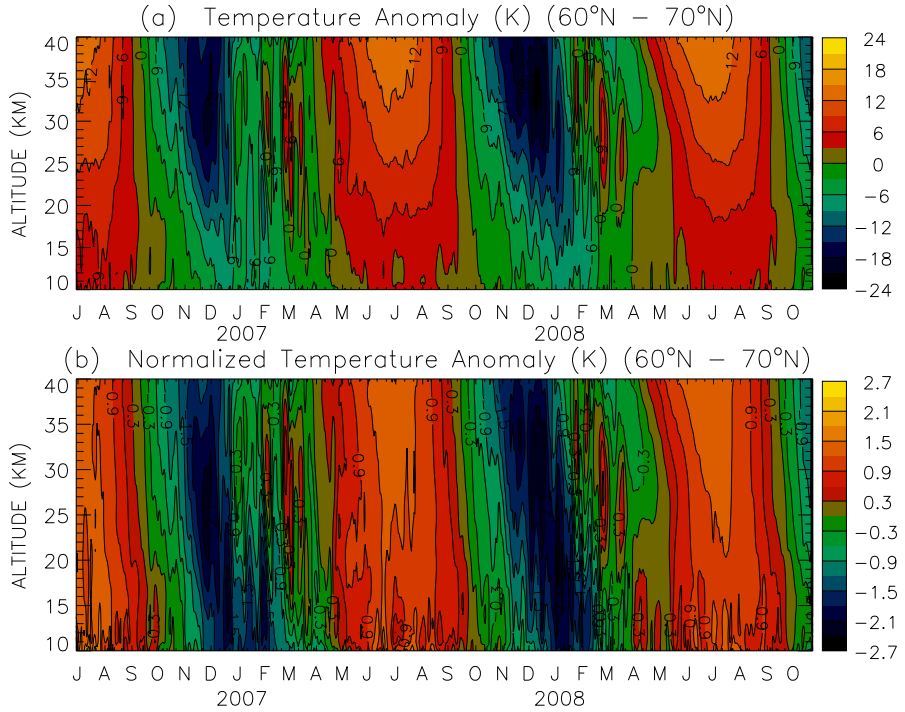

Fig. 1. (a) Temperature anomalies from the 28-month mean at 60° N–70° N and **(b)** normalized temperature anomalies.

ACPD
9, 14601–14643, 2009

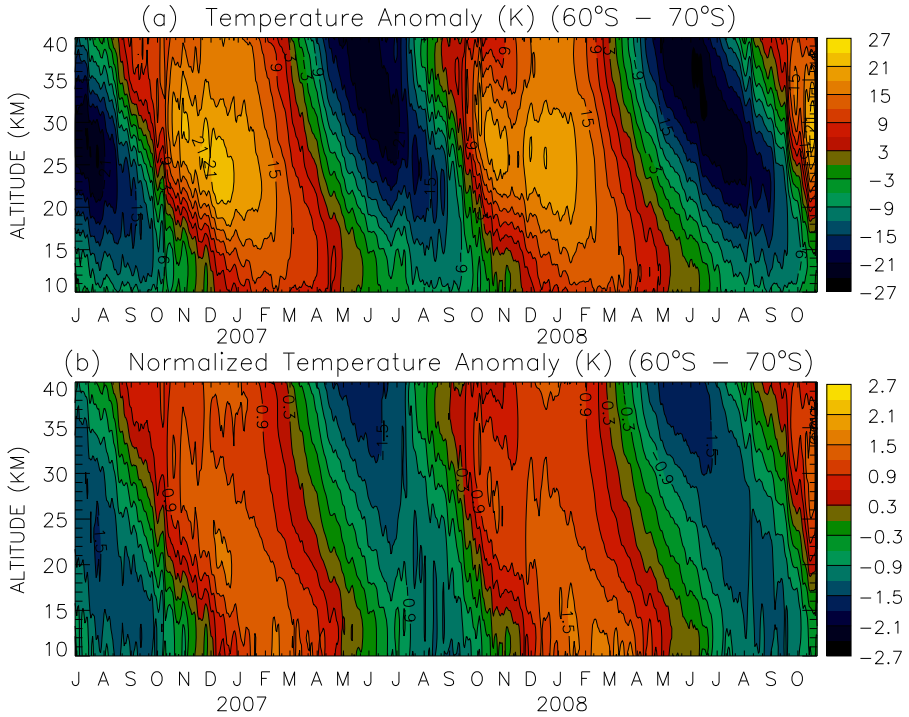

Fig. 2. Same as Fig. 1 but for 60° S–70° S.

ACPD
9, 14601–14643, 2009

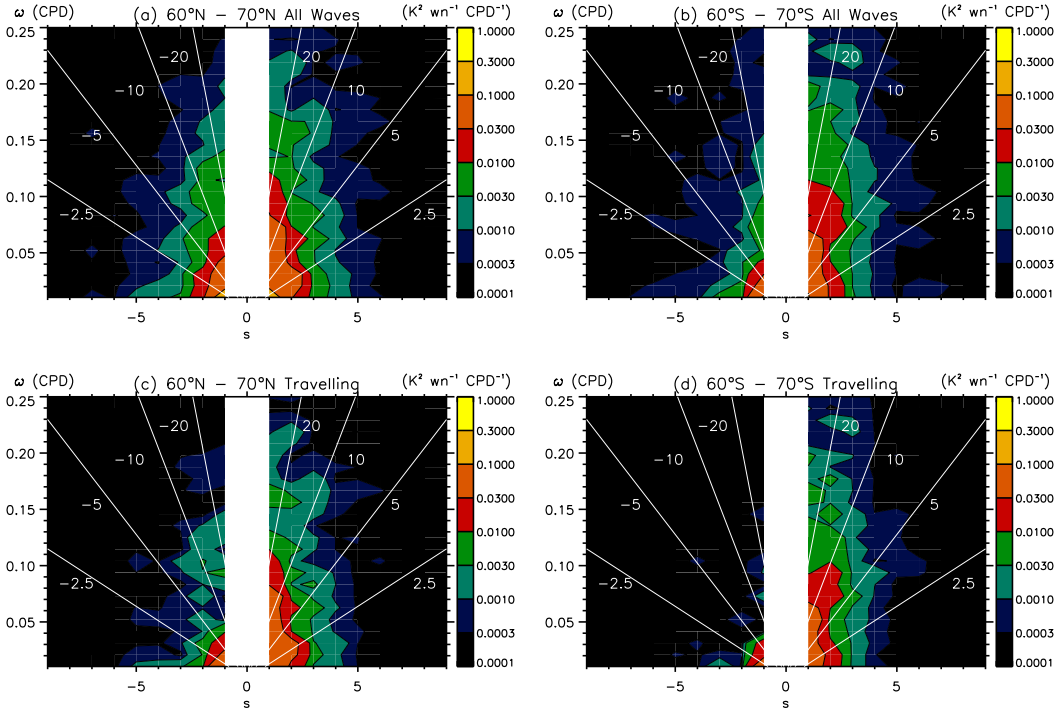

Fig. 3. *s–ω* spectra for the period 1 November 2006 to 4 November 2008 at 30 km altitude for 60° N–70° N (left hand column) and 60° S–70° S (right hand column). **(a, b)**: all wave components, **(c, d)** travelling components only. Negative *s* indicates westward propagation. White lines mark ground-based phase speeds (units m s^{-1}, positive eastward).

ACPD
9, 14601–14643, 2009

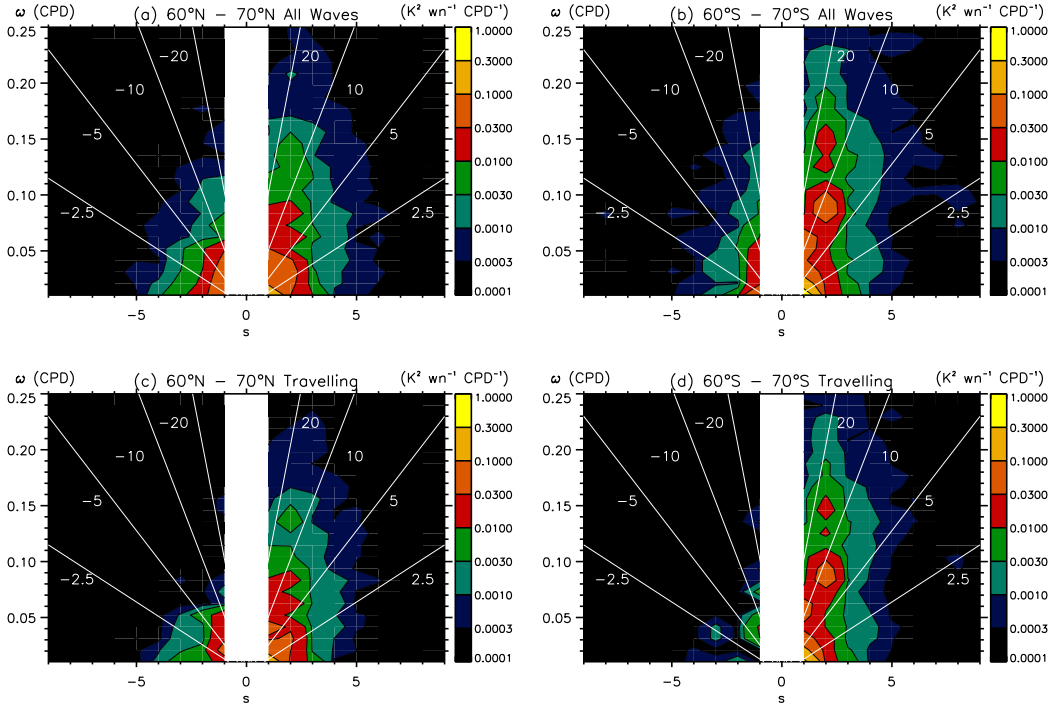

Fig. 4. Same as Fig. 3 except at 15 km altitude.

ACPD
9, 14601–14643, 2009

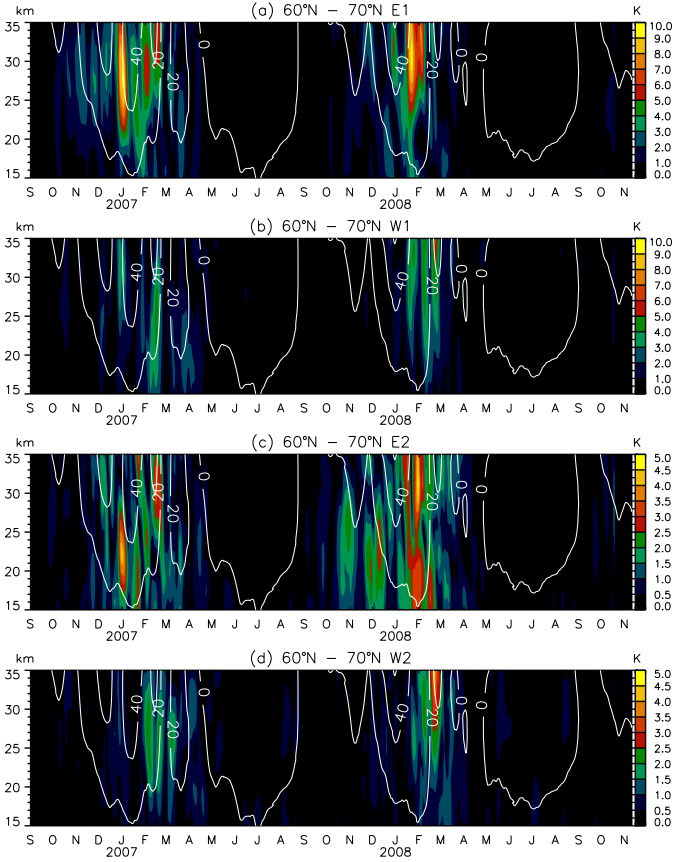

Fig. 5. The 60° N–70° N temperature amplitudes due to travelling planetary waves with discrete periods τ_j (see text for details): **(a)** E1, **(b)** W1, **(c)** E2, **(d)** W2. UKMO zonal mean zonal winds (white, units of m s^{-1}, solid eastward) are also marked.

ACPD
9, 14601–14643, 2009

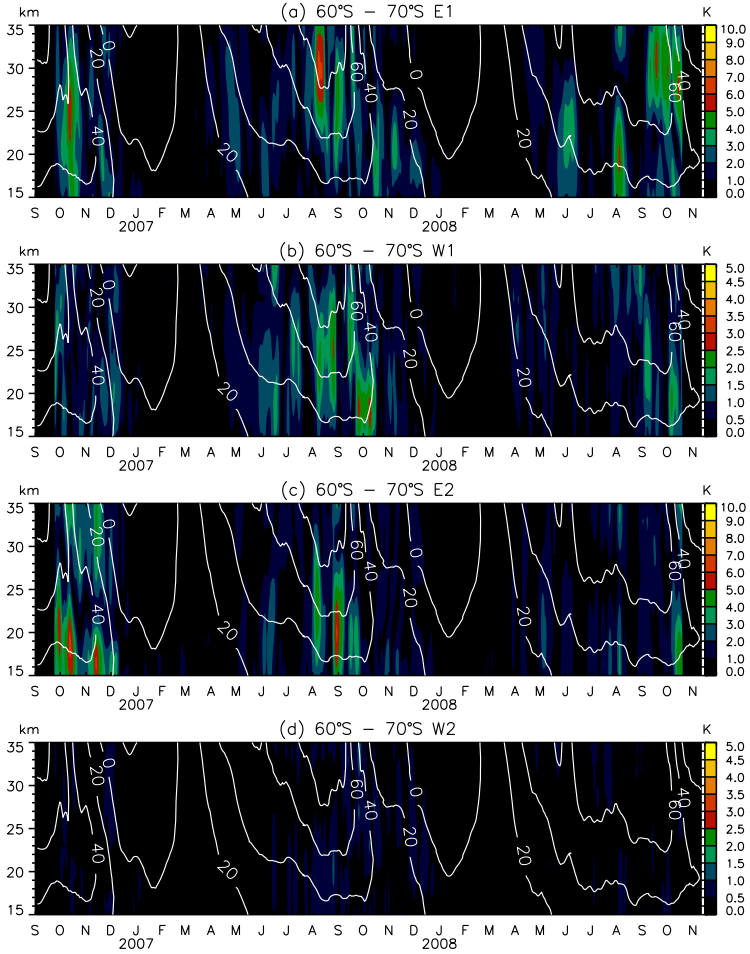

Fig. 6. As for Fig. 5 except at 60° S–70° S.

ACPD
9, 14601–14643, 2009

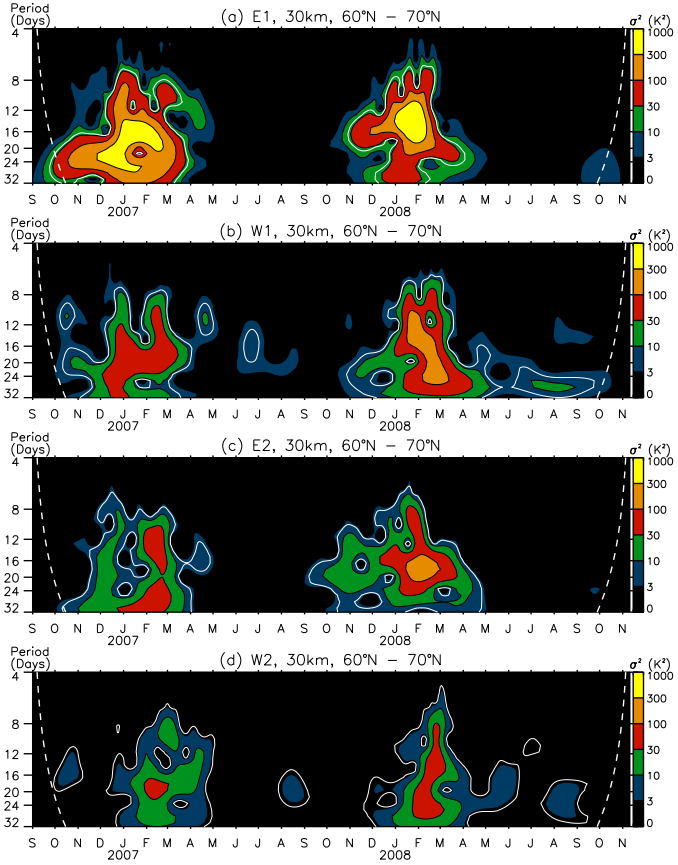

Fig. 7. Wavelet power spectrum for travelling planetary waves at 60° N–70° N: **(a)** E1, **(b)** W1, **(c)** E2, **(d)** W2. The 95% confidence lines are marked by the solid white lines, while the cones of influence are indicated by the white dashed lines (Torrence and Compo, 1998).

ACPD
9, 14601–14643, 2009

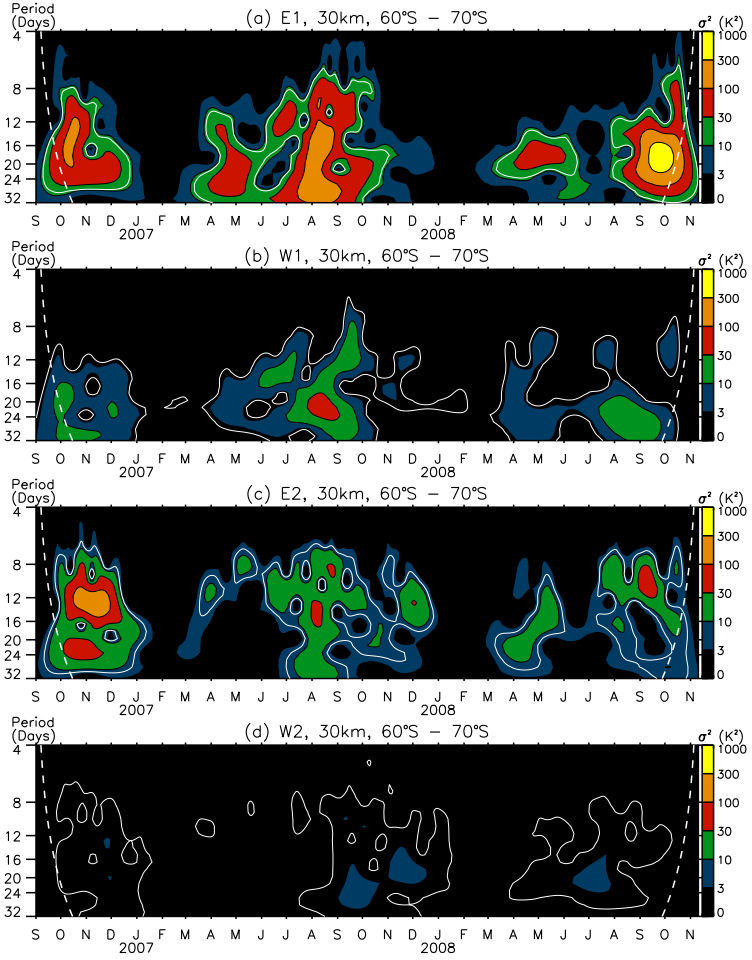

Fig. 8. As for Fig. 7 except at 60° S–70° S.

ACPD
9, 14601–14643, 2009

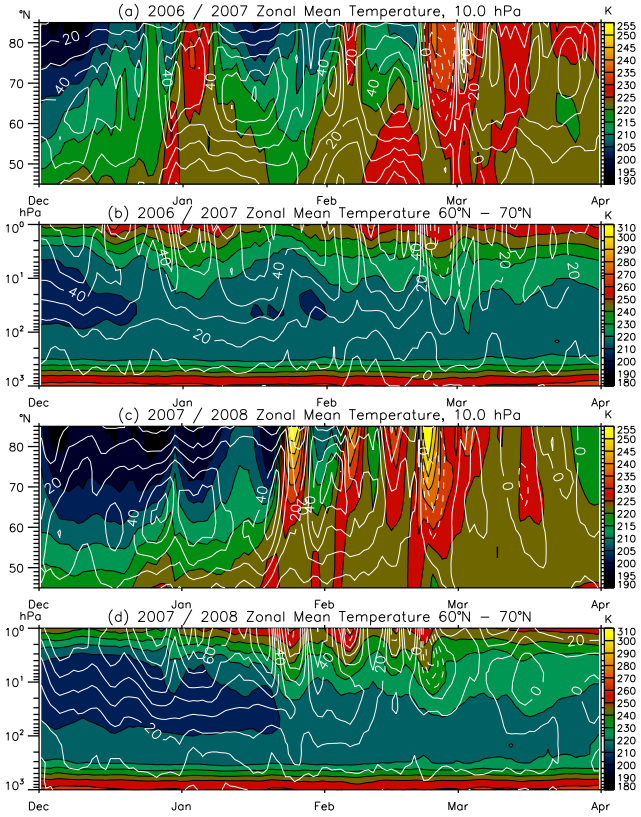

Fig. 9. Background state of the atmosphere during the Arctic winters of 2006/2007 and 2007/2008. **(a)** UKMO zonal mean temperature at 10 hPa (colour scale) with zonal mean zonal winds (white, units m s^{-1}, solid eastward) during 2006/2007; **(b)** zonal mean temperatures and zonal mean zonal winds at 60° N–70° N during 2006/2007; **(c)** same as (a) but for 2007/2008; (d) same as (b) but for 2007/2008.

ACPD
9, 14601–14643, 2009

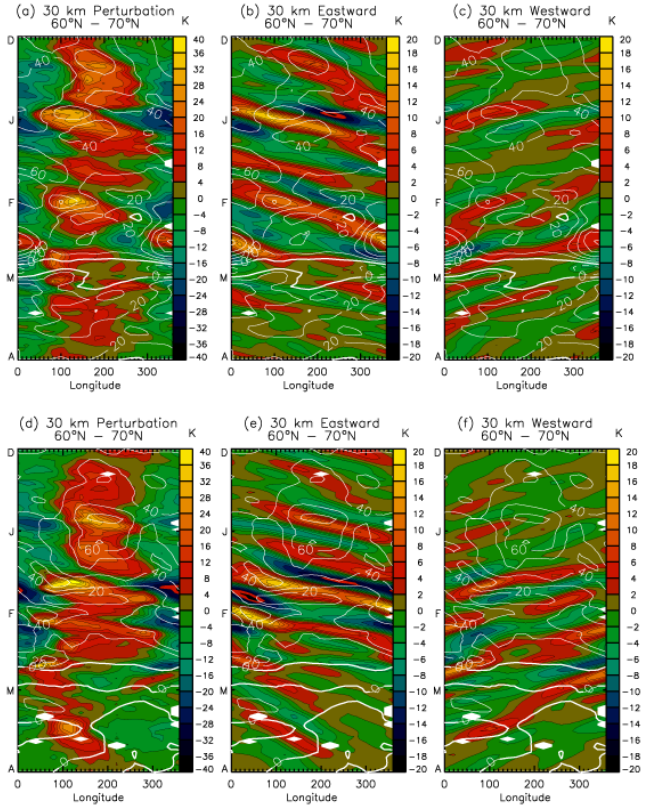

Fig. 10. Hövmoller diagrams at 60° N–70° N at 30 km during the Arctic winter of 2006/2007 (a–c) and 2007/2008 (d–f). **(a, d)** Temperature perturbation from zonal mean, **(b, e)** eastward propagating waves, **(c, f)** westward propagating waves. White indicates missing data. The five day smoothed UKMO zonal winds at the nearest pressure level (10 hPa) are marked in white (units m s^{-1}, solid eastward).

ACPD
9, 14601–14643, 2009

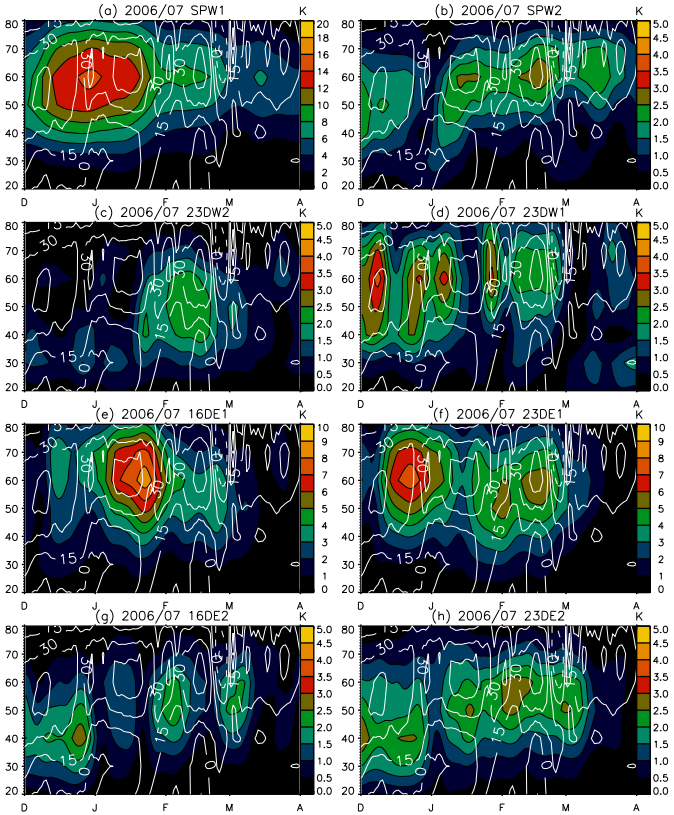

Fig. 11. Latitudinal distribution of planetary wave amplitudes in the Northern Hemisphere at 30 km during 2006/2007 winter, with the various waves labelled in the titles. Note the varying colour scales. The ordinate is latitude in degrees. The UKMO zonal mean zonal winds at 10 hPa are marked in white (units m s^{-1}, solid eastward and dashed westward).

ACPD
9, 14601–14643, 2009

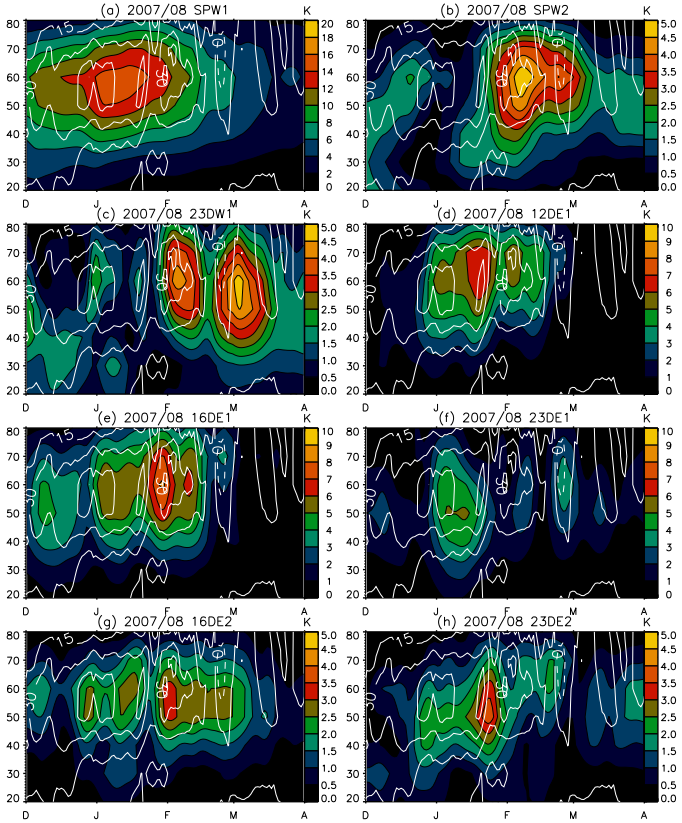

Fig. 12. As for Fig. 11 except for the 2007/2008 winter.

ACPD
9, 14601–14643, 2009

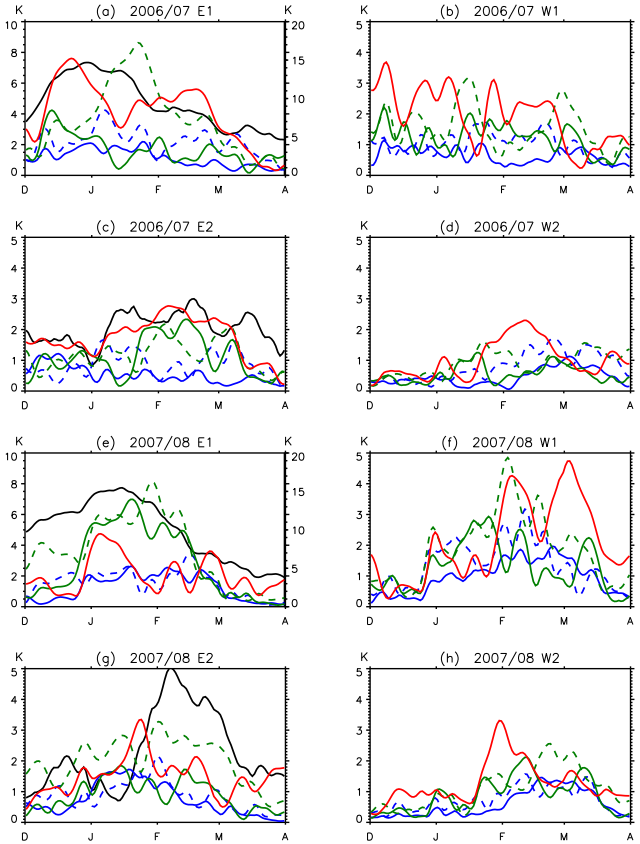

Fig. 13. Planetary wave amplitudes at 60° N–70° N and 30 km during the 2006/2007 winter **(a–d)** and during the 2007/2008 winter **(e–h)**. SPW are shown in black on the E1 and E2 plots (left hand column), with SPW1 using the scale to the right (a, e). The 8 day wave is marked dark blue (solid), the 10 day wave dark blue (dashed), the 12 day wave dark green (solid), the 16 day wave dark green (dashed) and the 23 day wave red.

ACPD
9, 14601–14643, 2009